Forum on Measurement Techniques in Multiphase Flows, 1995 ASME IMEC&E, November 1995, San Francisco, CA

DEVELOPMENT OF AN ELECTRICAL IMPEDANCE TOMOGRAPHY SYSTEM FOR AN AIR-WATER VERTICAL BUBBLE COLUMN*

T. J. O'Hern and J. R. Torczynski
Sandia National Laboratories
Albuquerque, New Mexico 87185

S. L. Ceccio and A. L. Tassin
University of Michigan
Ann Arbor, Michigan, 48109

G. L. Chahine, R. Duraiswami, and K. Sarkar
Dynaflow, Inc.
Fulton, Maryland 20759

ABSTRACT

Because the components of a multiphase flow often exhibit different electrical properties, a variety of probes have been developed to study such flows by measuring impedance in the region of interest. Researchers are now using electric fields to reconstruct the impedance distribution within a measurement volume via Electrical Impedance Tomography (EIT). EIT systems employ voltage and current measurements on the boundary of a domain to create a representation of the impedance distribution within the domain. The development of the Sandia EIT system (S-EIT) is reviewed. The construction of the projection acquisition system is discussed and two specific EIT inversion algorithms are detailed. The first reconstruction algorithm employs boundary element methods, and the second utilizes finite elements. The benefits and limitations of EIT systems are also discussed. Preliminary results are provided.

INTRODUCTION

The problem of measuring the spatial distribution of the separate phases in multiphase flows is one of great interest in a number of research and industrial applications (Plaskowski *et al.*, 1995). Diagnostic techniques typically applied to such measurements include radiation densitometry and tomography such as gamma tomography, positron emission tomography (PET), and magnetic resonance imaging (MRI) (Kumar *et al.*, 1994; Shollenberger *et al.*, 1995; Simons, 1995). These techniques offer high spatial resolution. However, radiation tomography often requires significant data collection times, which are usually much longer than the characteristic time scales of a temporally evolving multiphase flow. Electrical impedance measurements can be acquired relatively fast and have been used for some time to measure bulk and local void fractions (Ceccio and George, 1995). However, the spatial resolution of electrical probes is limited. Electrical impedance tomography (EIT) may offer a method to quickly acquire images of the spatial distribution of phases within a multiphase flow. EIT is the process by which electrical measurements, acquired at the boundary of a domain, can be used to reconstruct the electrical impedance distribution within the domain (Webster, 1990; Plaskowski *et al.*, 1995; Jones *et al.*, 1993). In this paper, we will detail an EIT system being constructed at Sandia National Laboratories for the purpose of investigating multiphase bubble column reactors, such as Fischer-Tropsch reactors. Slurry-phase bubble-column Fischer-Tropsch reactors are recognized as one of the more promising technologies for indirect liquefaction, *i.e.*, converting synthesis gas from coal into liquid fuel products (see, *e.g.*, Bukur *et al.*, 1987). However, hydrodynamic effects must be considered when attempting to scale these reactors to sizes of industrial interest. Development and application of noninvasive tomographic diagnostics capable of measuring void fraction (gas holdup) spatial distributions in these reactors would greatly facilitate characterization of reactor hydrodynamics.

We will discuss the experimental setup, including design aspects of the EIT hardware, reconstruction algorithms under development, and some preliminary results.

BASICS OF ELECTRICAL IMPEDANCE TOMOGRAPHY

EIT is a technique by which the impedance distribution within a domain may be determined via voltage and current measurements performed on the boundary of the domain. For AC electrical conduction with field frequencies on the order of tens of megahertz or lower, the electrical potential within a conducting domain, Ω, is given by

$$\nabla \cdot \sigma \nabla \phi = 0 \qquad (1)$$

*This work was performed at Sandia National Laboratories, supported by the U.S. Department of Energy, under contract DE-AC04-94AL85000.

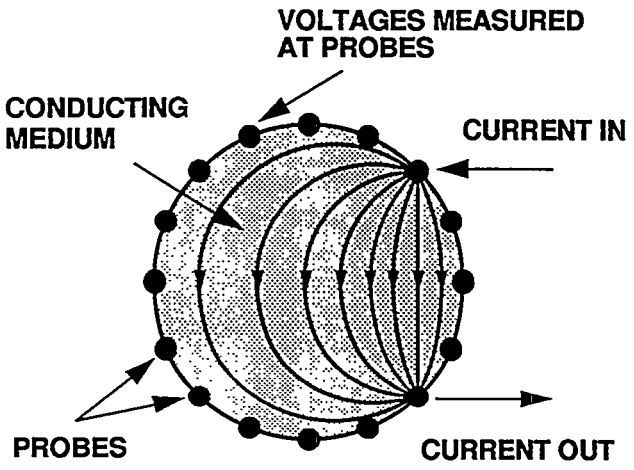

Figure 1. Schematic diagram of an EIT setup.

when no charge sources or sinks are present in Ω. Here, σ is the complex conductivity and ϕ is the electrical potential. At the boundary of Ω, the mixed boundary conditions are given by

$$\sigma \nabla \phi \cdot \mathbf{n} + \sum q = 0 \qquad (2)$$

where **n** is the unit normal vector outward from the domain boundary, and $\sum q$ represents sources and sinks of charge on the boundary. In EIT, multiple measurements of q and ϕ at the boundary of Ω are used to reconstruct the conductivity distribution within Ω. An iterative reconstruction process is required to arrive at a conductivity distribution which will yield the measured boundary conditions.

In practice, the injection of current at the domain boundary and the measurements of voltage at the domain boundary will be conducted at a finite number of locations on the boundary, and these measurements may be averaged over a portion of the boundary surface. Consequently, the resolution of the reconstruction of the conductivity field will be limited, and the resolution will be strongly related to the number of ports used to probe the domain.

A finite number of electrodes will be used to both inject charge into the domain and measure voltages at the boundary (Figure 1). If M electrodes are used, the domain can be modeled as an M port impedance network. If a current source and current sink of equal strength are placed on two of the ports, the resulting voltage distribution around the "network" can be measured at (M-1) ports, with one port referenced to ground. The total number of linearly independent voltage measurements, N_E, is then given by

$$M(M\text{-}1)/2 = N_E \qquad (3)$$

N_E is the number of independent impedances which can be determined from these "projections." Thus, the domain can de divided into a maximum of N_E impedance elements, and the spatial resolution will be approximately proportional to M^2.

EIT imaging of multiphase flows is possible if a significant difference exists between the complex conductivity of the various phases within the domain to be imaged. For aqueous systems with field frequencies below a few megahertz, the real part of the complex conductivity dominates. For dielectric systems, such as hydrocarbons, the complex part of the conductivity dominates, and the conductivity of air is almost completely complex. Thus, air/water and hydrocarbon/water systems offer strong potential for EIT. Hydrocarbon/air systems are more difficult, as the difference on the complex conductivity of the two systems is small, and higher field frequencies are needed to detect differences in the two phases. Also, it is possible to detect the presence of more than two phases, if the electrical properties of the multiple phases are sufficiently different.

EXPERIMENTAL TECHNIQUES

Bubble Column

An air-water bubble column has been assembled for examination of the EIT technique under dynamic conditions (see Figure 2). The lucite bubble column has a 0.19 m inner diameter and is 1.8 m tall. Gas is introduced through one of several interchangeable distributors (spargers) located at the base of the column. Monitoring the change in liquid level with a high speed video camera has been used to determine the average void fraction in the air-water column over a range of gas flowrates, or superficial gas velocities (the velocity of gas if it filled the flow cross-sectional area). During steady air flow, the volume-averaged void fraction can be determined according to $H_0/(H_0+\Delta H)$, where H_0 is the height of the water with no air flow and ΔH is the change in height during air flow. To date, gas holdups up to 0.4 have been observed for air flow rates up to 600 liter/min and superficial velocities as high as 35 cm/s.

Bulk Impedance Void Fraction Meter

A dual-electrode impedance void fraction meter was implemented to measure the average and time-varying bulk void fraction across a section of the bubble column. The electrodes are 3.8 cm tall in the axial (flow) direction, and subtend a 120 degree angle. A sinusoidal excitation current of frequency 50 kHz was applied to the electrodes. The size and shape of the electrodes determines the electric field lines in the fluid, and therefore the volume over which the void fraction is averaged. Such a simple void fraction meter can be calibrated to measure void fraction in the bubbly and churn flow regimes. The void fraction meter was calibrated with level-rise, differential pressure, and gas flow rate. The device calibrated well with these techniques.

Electrical Impedance Tomography

Figure 3 shows a block diagram of the EIT system currently being constructed for Sandia (S-EIT). The system consists of a signal generator, a voltage controlled current source, multiplexers to and from the electrode array, an instrumentation amplifier, phase sensitive demodulators, and a digital controller.

The S-EIT sources and sinks current at two ports, and voltages are measured at all ports relative to the sinking port. In an ideal system, no additional information may be gained by injecting current at more than two ports, and any pattern of electrode pairs may be used to measure boundary voltages. In such a system, the domain under study is modeled as an impedance network. In practice, however, different projection techniques may yield different

DISCLAIMER

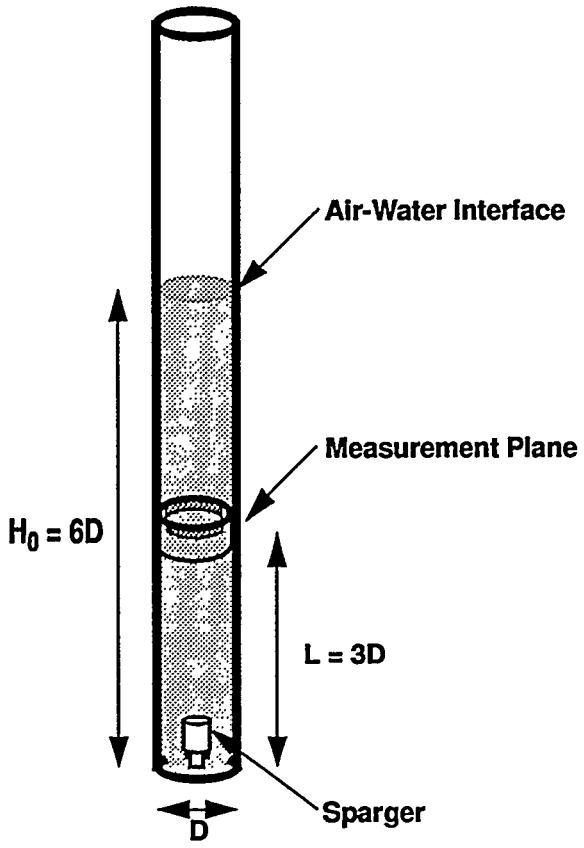

Figure 2. Schematic diagram of air-water bubble column used for EIT and bulk impedance measurements. Measurement plane at L/D=3.

results. Some schemes have been devised to increase resolution near the boundary of the domain, while other schemes have been devised to improve resolution within the domain. To acquire a set of projections with good signal to noise ratio, significant current should be induced within the entire domain of interest so as to detect measurable changes in the boundary voltages.

The domain under study will be probed with an AC electric field. The frequency of the field which will be imposed by the S-EIT will be between 50 and 100 kHz, a frequency range acceptable for air/water systems. The injection current will be created with a voltage controlled current source (VCCS) employing two operational amplifiers in a positive feedback design. The approximate range of domain impedances should be known in order to prevent saturation of the VCCS due to extremely high domain impedances.

The electrode array is connected to the current source and sink via analog multiplexers (MUXs). MUXs are also used to connect the electrode array to the differential amplifier used to measure electrode voltages. Coaxial cable is used to carry the injection current to and from the electrodes surrounding the domain, and the shields of the cable are brought to the electrode voltage with voltage followers. A separate set of cables will be used to connect the electrodes to the voltage MUXs to prevent the inclusion of any voltage drop which may occur across the current lines, and the

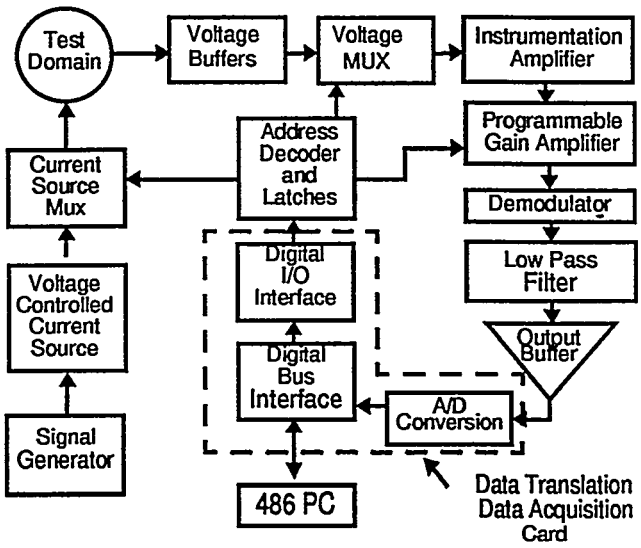

Figure 3. Block diagram of EIT hardware.

voltages on each electrode are buffered with a single operation amplifier. These voltage signals are passed to a differential amplifier which is used to measure the difference between the voltages on two electrodes. The differential amplifier must have a good common mode rejection ratio (CMMR) and allow the measurement of voltage differences over a wide dynamic range.

The signal from the differential amplifier is demodulated with a phase sensitive demodulator (PSD). Two demodulators are used to recover the in-phase and quadrature portion of the signal amplitude. The in-phase and quadrature demodulator output is low pass filtered with a cutoff frequency of 25 kHz. The two voltage outputs of the PSD are then buffered and passed to the analog to digital converter on the digital controller board. A digital controller is used to select the current injection electrodes and perform the voltage measurements as well as acquire the demodulated signal levels. An analog/digital interface is used to connect a PC to the S-EIT system.

The S-EIT system will employ 16 electrodes, and the domain to be probed will be a cylindrical section. The shape and placement of the electrodes on the domain boundary will have a significant influence on the resolution of the EIT system. The electrodes will be equally spaced around the circumference of the domain. The choice of the individual electrode geometry requires some compromise. It is desirable to have electrodes with small surface areas (point electrodes) to approximate point sources of current. Electrodes with finite size will not emit current uniformly over their surface, and this may induce errors in the reconstruction if these "near field" effects are not dealt with. However, voids in a distributed multiphase system may completely cover a point electrode and eliminate almost all of the current flow within the domain. Thus, for the S-EIT system, electrode strips of approximately 1% of the circumference were chosen as a compromise. Next, the length of the electrodes was determined. If point electrodes are used, the lines of current flux will not be confined to a plane across

the domain. Instead, the current lines will "bulge out" near the middle of the domain, and a large volume of the domain center will be probed. The S-EIT system currently employs electrodes which are rectangular strips with aspect ratio of 12:1. Thus, a volume of the domain will be probed, the influence of the field "end effects" will be minimized. Of course, the reconstructed image will be a volume average of the domain.

EIT RECONSTRUCTION TECHNIQUES

The methodology, accuracy and efficiency of EIT tomographic reconstruction algorithms continues to be a subject of research (Yorkey *et al.*, 1987; Hua and Woo, 1990; Jones *et al.*, 1993; and Ceccio and George, 1995). EIT algorithms can be grouped broadly in terms of the problem dimensionality (2 or 3), the impedance model employed (*e.g.*, resistive, capacitive), the numerical method used to discretize the equations (*e.g.*, finite element method, boundary element method), the representation of the impedance field (*e.g.*, piecewise constant, exponential), the means by which the impedance field is modified during an iteration (*e.g.*, back-projection between equipotential lines, Newton-Raphson), and, of course, the intended application (*e.g.*, biomedical imaging, multiphase flow measurement). Two distinct EIT reconstruction algorithms are being developed for the S-EIT, one based on the boundary element method and the other based on the finite element method.

Boundary Element Methods for EIT Reconstruction

Solution of an electric impedance computed tomography problem using a Boundary Element Method (BEM) would have the invaluable advantage of considerably reducing computational time, especially for three-dimensional problems. Indeed, by requiring discretization of only the boundary, the BEM reduces the dimension of the problem by one, and leads to orders of magnitude reduction in memory and CPU time requirements. Because this is a relatively new reconstruction technique, a detailed description is provided here.

Consider a set of N_E experiments where, using M electrodes, we impose known voltages at M selected points on the boundary S of a domain Ω and measure the resulting current (or vice-versa). From these measurements we want to determine the electric conductivity of the medium, σ. The electric potential, ϕ, satisfies the following equation:

$$\nabla \cdot \sigma \nabla \phi = 0 \text{ in } \Omega \tag{4}$$

subject to the boundary conditions

$$\begin{cases} \dfrac{\partial \phi}{\partial n} \text{ and } \phi \text{ measured at the electrodes} \\ \dfrac{\partial \phi}{\partial n} = 0 \text{ on the rest of the boundary} \end{cases} \tag{5}$$

A direct method for obtaining σ from such measurements is not readily available. Instead, starting from a guessed distribution of σ, a "*forward problem*" is solved. Then, minimization of the error between the predicted and the measured values of ϕ on the boundary is sought for the next guess of the σ distribution, and the procedure is repeated until satisfactory convergence is achieved.

If the domain to be imaged contains materials which have vanishing conductivity (*e.g.*, air bubbles in a conducting liquid), the problem with the same boundary conditions (5) simplifies to:

$$\nabla^2 \phi = 0 \text{ in } (\Omega - \text{Inclusions}) \tag{6}$$

with the additional boundary condition $\partial\phi/\partial n = 0$ on the surface of the inclusions.

As presented below both equations (4) and (6) can be reformulated via the following Green's identity:

$$a\pi\phi(x) = \int_V \nabla_y^2 \phi(y)\, G(x,y)\, dV + \int_S n_y \bullet [\phi(y) \nabla_y G(x,y) - G(x,y) \nabla_y \phi(y)]\, dS \tag{7}$$

where the Green function, G, is the fundamental solution to Laplace's equation. The quantity $a\pi$ is the angle (in 2D) or the solid angle (in 3D) under which point x "sees" the conducting domain. For the case of a medium containing vanishing conductivity inclusions, Laplace's equation (6) applies and the volume integral in Equation (7) vanishes. The resultant boundary integral equation can be solved by following a collocation approach and selecting the points x on the boundary S. A linear system of equations results, and is of the form:

$$A\left\{\frac{\partial \phi}{\partial n}\right\} = B\{\phi\} \tag{8}$$

where the matrices A and B correspond to the discretization and integration with the Green's function and its derivative. The solution of this system of equations provides the values of ϕ and $\partial\phi/\partial n$ at the boundary (Chahine and Perdue, 1989; Chahine and Duraiswami, 1994) and therefore enables evaluation of the errors resulting from the guessed position and geometry of the vanishing conductivity medium inside the domain Ω.

More generally, Equation (4) can be rewritten as a Poisson equation:

$$\nabla^2 \phi = b(x) = -(\nabla \log\sigma \bullet \nabla\phi)(x) \tag{9}$$

In order to eliminate the volume integral term from the Green's identity reformulation of (9), we follow the dual reciprocity method (Partridge *et al.*, 1992), and express both b and ϕ in terms of a special set of known basis functions $\{f_j\}$.

$$b(x) = \sum_{j=1}^{\infty} \alpha_j f_j(x), \text{ and } \phi = \sum_{j=1}^{\infty} \beta_j f_j(x) \tag{10}$$

Corresponding to each function $\{f_j\}$ there exists another known function $\{\psi_j\}$ related to it by:

$$\nabla^2 \psi_j = f_j \tag{11}$$

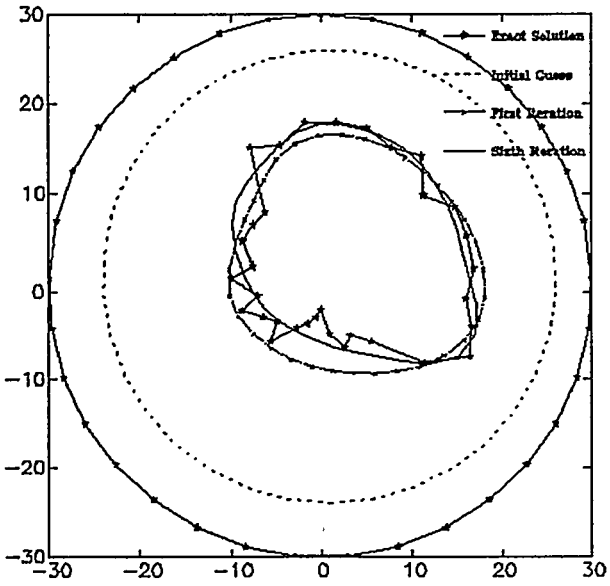

Figure 4. Detection of a noncircular body using the 2D BEM code. Fast approximate convergence is achieved using a Legendre polynomial description of the body and the Powell's direction set minimization method.

Practically, the summations are restricted to M terms, and the vectors of coefficients α_j and β_j are connected to the vectors b and ϕ by the matrix equations:

$$\alpha = \mathbf{F}^{-1} b \qquad \beta = \mathbf{F}^{-1}\phi. \tag{12}$$

The third Green's identity becomes after using Expansion (10) for $b(\mathrm{x})$:

$$a\pi\phi = \int_S \left(\phi\frac{\partial G}{\partial n} - G\frac{\partial \phi}{\partial n}\right) dS + \sum_{j=1}^{M} \alpha_j \left[\psi_j(x) - \int_S \left(\psi_j \frac{\partial G}{\partial n} - G\frac{\partial \psi_j}{\partial n}\right) dS\right] \tag{13}$$

where the domain term in (7) has been reduced to a boundary-only formulation. This can be written, after collocation:

$$\mathbf{B}\{\phi\} - \mathbf{A}\{\frac{\partial \phi}{\partial n}\} = \left(\mathbf{B}\{\psi\} - \mathbf{A}\{\frac{\partial \psi}{\partial n}\}\right)\mathbf{F}^{-1}\mathbf{b} \tag{14}$$

Similarly using the expansion for ϕ, b can be evaluated as:

$$\mathbf{b} = \left(\frac{\partial k}{\partial x}\frac{\partial \mathbf{F}}{\partial x}\mathbf{F}^{-1} + \frac{\partial k}{\partial y}\frac{\partial \mathbf{F}}{\partial y}\mathbf{F}^{-1} + \frac{\partial k}{\partial z}\frac{\partial \mathbf{F}}{\partial z}\mathbf{F}^{-1}\right)\phi \tag{15}$$

where k=log σ. After substitution of b by its expression (15), Equation (14) becomes

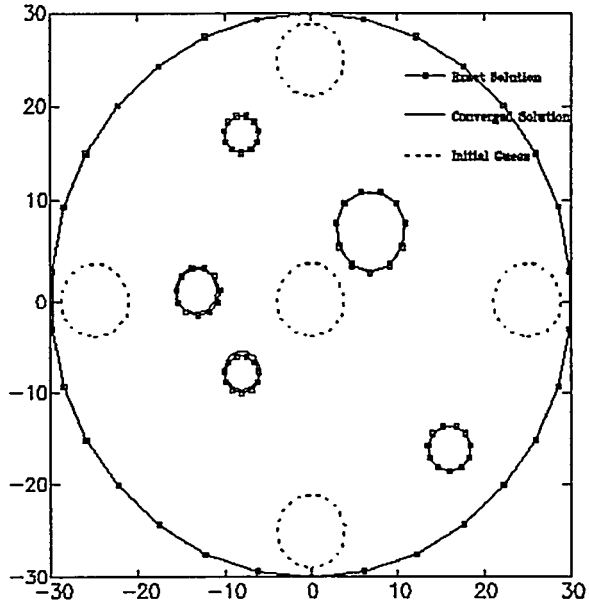

Figure 5. Detection of a five circular inclusions using the 2D BEM code.

$$\mathbf{A}\{\frac{\partial \phi}{\partial n}\} = |\mathbf{B} - \mathbf{S}(k)|\{\phi\} \tag{16}$$

where

$$\mathbf{S} = (\mathbf{B}\psi - \mathbf{A}\eta)\mathbf{F}^{-1}\left(\Lambda_{kx}\frac{\partial \mathbf{F}}{\partial x}\mathbf{F}^{-1} + \Lambda_{ky}\frac{\partial \mathbf{F}}{\partial y}\mathbf{F}^{-1} + \Lambda_{kz}\frac{\partial \mathbf{F}}{\partial z}\mathbf{F}^{-1}\right) \tag{17}$$

Λ_{kx} represents a diagonal matrix containing the values of the quantity $\partial k/\partial x$ at the points at which the domain term is collocated.

There are a number of functions f_j available to perform the dual-reciprocity expansions. One particular set that we have used is the "*radial function*" which is based on the distance between the collocation point and the point of interest,

$$f_j(x) = 1 + |x_j - x|. \tag{18}$$

These distances have the advantage of being also needed in the BEM computations to evaluate the Green's function which involves $|x_j - x|$.

The inverse problem consists of finding out through a minimization procedure a set of unknowns, here either the shape and position of inclusions or parameters describing the distribution of conductivity in the domain. We can then use one of the existing multi-dimensional minimization schemes. To date we have tried three methods: the downhill simplex method, the direction set or Powell's method, and the conjugate gradient method (Press *et al.*, 1992). All were found to converge quite satisfactorily.

For the 2D case of two cylindrical inclusions of zero conductivity inside a cylindrical container, a systematic comparison

between the three methods shows that the downhill simplex method requires the least number of evaluations of the error, *i.e.* the least number of computations of the forward problem to lead to an extremely small rms error. However, in a practical application where the position and the radius of the sought inclusion are only required within a reasonable amount of precision, the Powell method appears to have the fastest initial convergence rate. For instance, in 2D for a single noncircular body, the Powell method gives a satisfactory approximation at the first iteration. Here, the shape is described using 13 unknowns, the (x, y) position of the center of the shape, and 11 Legendre polynomial coefficients. Convergence in that case takes only a few minutes on an SGI Indigo workstation. Figure 5 shows the case of five circular inclusions. An excellent convergence can be seen for an initial arbitrary guess also shown on the figure.

Finite Element Methods for EIT Reconstruction

Following the basic approach of Yorkey *et al.* (1987), an EIT reconstruction algorithm using the finite element method (FEM) and Newton-Raphson iteration has been implemented. This is a relatively well-known reconstruction method, and therefore will only be briefly detailed here. The problem is treated as strictly two-dimensional, and the medium is treated as purely resistive (no capacitive contribution), which is reasonable for the air-water systems of interest here. Equation 4 is discretized using the Galerkin finite element method, and the electrical conductivity is represented as a linear combination of the products of conductivity fitting parameters with functions of position. The Newton-Raphson method is used to update these parameters during each iteration so as to minimize the rms error between the measured and computed voltages. In this approach, the EIT probes are assumed to be small in width compared with their separations, so current-bearing probes are treated as two-dimensional point sources/sinks. As a result, the voltages at current-carrying probes are not used in the least-squares fit. Furthermore, since all the boundary conditions are of the Neumann form, an interior node is selected and specified to have zero voltage for all experiments, and a constant voltage offset per experiment is included as an unknown adjustable parameter (and treated in the same manner as the conductivity parameters).

The resulting finite element method electrical impedance tomography (FEMEIT) algorithm can be summarized as follows. Specify the voltage mesh (*i.e.* element type, nodes, elements, shape functions) and the conductivity functions (which are generally of large extent compared with the voltage elements). Precompute (once for all) the partial global stiffness matrices, which are the contributions to the total global stiffness matrix from each conductivity function. The iteration loop consists of computing the total stiffness matrix (based on the particular values of the conductivity parameters), inverting this matrix, using this inverse to find the voltages at each probe and the corresponding Jacobian terms necessary for the Newton-Raphson algorithm for all possible pairwise combinations of current-carrying probes, and solving the (linearized) least-squares problem to minimize the rms voltage difference. Iterations proceed until appropriate tolerances are satisfied.

A computer code has been written to implement this approach. This code treats general two-dimensional regions, including multiply connected regions, and both perimeter and internal probes. Linear triangle elements are used to construct the partial global stiffness matrices. Since probes are represented as mathematical points, a node must be placed at each probe. The conductivity functions are selected from a library of choices in a subroutine (*e.g.* Cartesian polynomials, radial polynomials).

Two types of validation calculations have been performed. The first type involves using the analytical result for the voltage distribution in a constant-conductivity circular domain. The second involves using the finite-element code FIDAP (Fluid Dynamics International, 1995) to compute the voltages that would be observed with a 16-probe EIT device for a certain prescribed electrical conductivity spatial distribution, shown in Figure 6. Also shown in Figure 6 is the reconstructed conductivity field produced by the previously discussed algorithm, where the conductivity functions are chosen to be linear combinations of the following functions: $1, x, y, x^2, xy, y^2, x^3, x^2y, xy^2, y^3, x^4, x^3y, x^2y^2, xy^3, y^4$. FIDAP has been used to post-process the FEMEIT result. Agreement is seen to be good.

RESULTS AND CONCLUSIONS

The EIT system has been applied for measurements in the air-water bubble column over a range of gas injection flow rates. To date, we are still developing our tomographic system, but we have been able to measure the bulk void fraction based on the assumption of a homogeneous bubbly mixture. Figure 7 shows the measured void fraction vs. gas flowrate as determined by five different measurement techniques: differential pressure measurement, optical detection of the free surface level rise, the bulk void fraction meter, gamma ray tomography, and the electrical impedance tomograph. The comparison between these techniques is reasonable.

The next step in our EIT development will be to optimize the electrode configuration and compare measured projections of the homogeneous domain (no gas flow) to analytical/numerical predictions. Simultaneous to this will be the further development of the reconstruction algorithms, including tests using analytically-derived "phantoms." We will also test for convergence and sensitivity to noise.

ACKNOWLEDGMENTS

The authors gratefully acknowledge the efforts of Kim Shollenberger and Tom Grasser of Sandia National Laboratories; Kim for her assistance in running the bubble column experiments and Tom for his hard work in assembling the EIT electrodes and the bubble column. This work was performed at Sandia National Laboratories, supported by the U. S. Department of Energy under contract number DE-AC04-94AL85000. The support of DOE/Sandia Laboratory-Directed Research and Development (LDRD) funds is gratefully acknowledged.

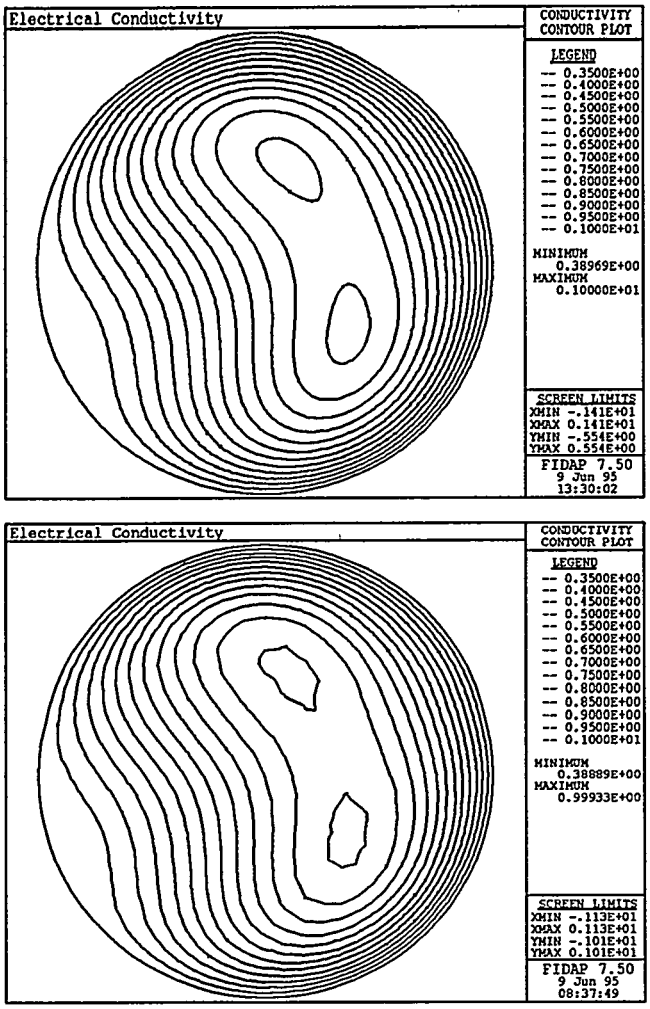

Figure 6. Top: specified electrical conductivity used by FIDAP. Bottom: electrical conductivity reconstructed by FEMEIT.

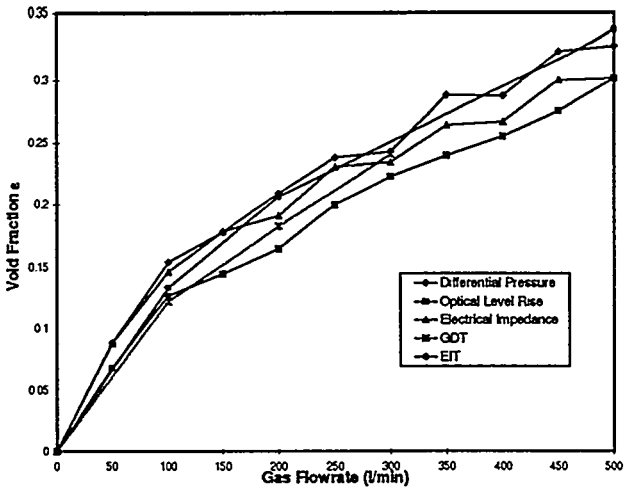

Figure 7. Bulk impedance in air-water bubble column as determined by various techniques.

REFERENCES

Bukur, D. B., Patel, S. A., and Matheo, R., 1987, "Hydrodynamic Studies in Fischer-Tropsch Derived Waxes in a Bubble Column," *Chem. Eng. Comm., 60*, 63-78.

Ceccio, S. L., and George, D. L., 1995, "A Review of Electrical Impedance Techniques for the Measurement of Multiphase Flows," *J. Fluids Engr.*, accepted for publication.

Chahine, G. L. and Perdue, T. O., 1989, "A 3D Boundary Element Method for Explosion Bubble Dynamics," in Drops and Bubbles, T.G. Wang, ed., *A.I.P. Conference Proceedings, 197*, 169-187.

Chahine, G. L. and Duraiswami, R., 1994, "Boundary Element Method for Calculating 2D and 3D Underwater Explosion Bubble Behavior in Free Water and Near Structures," *Report NSWCDD/ TR-93/44*, Naval Surface Warfare Center, Dahlgren Div., White Oak Detachment.

Fluid Dynamics International, 1994, FIDAP Users Manual, Fluid Dynamics International, Evanston, IL.

Hua, P., and Woo, E. J., 1990, "Reconstruction Algorithms," Electrical Impedance Tomography, J. G. Webster, ed., Adam Hilger, Bristol and New York, Chapter 10.

Jones, O. C., Lin, J.-T., Ovacik, L., and Shu, H.-J., 1993, "Impedance Imaging Relative to Gas-Liquid Systems," *Nuclear Engineering and Design, 141*, 159-176.

Kumar, S. B., Moslemian, D., and Dudukovic, M. P., 1994, "A γ-ray Tomographic Scanner for Imaging Voidage Distribution in Two-Phase Flow Systems," *Flow Meas. Instrum., 5*.

Partridge, P. W., Brebbia, C. A., and Wrobel, L. C., 1992, The Dual Reciprocity Boundary Element Method, Elsevier, London.

Plaskowski, A. Beck, M. S., Thorn, R., and Dyakowski, T., 1995, Imaging Industrial Flows: Applications of Electrical Process Tomography, Institute of Physics Publishing, London.

Press, W. H., Teukolsky, S. A., Vettterling, W. T. and Flannery, B. P., 1992, Numerical Recipes, Cambridge University Press, 2nd ed.

Shollenberger, K. A., Torczynski, J. R., Adkins, D. R., and O'Hern, T. J., "Bubble Column Measurements Using Gamma Tomography," G. Morrison, ed., *Proc. ASME Fluid Measurements and Instrumentation Forum*.

Simons, S. J. R., 1995, "Imaging Techniques for Fluidized Bed Systems: A Review," *Chem. Eng. J., 56*, 83-93.

Webster, J. G., ed., 1990, Electrical Impedance Tomography, Adam Hilger, New York.

Yorkey, T. J., Webster, J. G., and Tompkins, W. J., 1987, "Comparing Reconstruction Algorithms for Electrical Impedance Tomography," *IEEE Transactions on Biomedical Engineering, BME-34*, 11, 843-852.